APL Materials

RESEARCH ARTICLE | JULY 18 2017

High mobility yttrium doped cadmium oxide thin films

Kyle P. Kelley ; Edward Sachet; Christopher T. Shelton; Jon-Paul Maria

APL Mater. 5, 076105 (2017)
https://doi.org/10.1063/1.4993799
CHORUS

High mobility yttrium doped cadmium oxide thin films

Kyle P. Kelley, Edward Sachet, Christopher T. Shelton, and Jon-Paul Maria
Department of Materials Science, North Carolina State University, Raleigh, North Carolina 27695, USA

(Received 23 May 2017; accepted 29 June 2017; published online 18 July 2017)

Donor doped CdO thin films on *c*-plane sapphire are prepared by reactive co-sputtering from Cd-metal and Y-metal targets which are driven using pulsed-dc and RF power respectively. Intrinsic CdO exhibits a carrier density of 1.8×10^{19} cm^{-3} and a mobility of 330 cm^2 V^{-1} s^{-1}. By increasing the Y-flux, carrier density values can be increased smoothly and reproducibly to a maximum value of 3.3×10^{20} cm^{-3}. Mobility increases with Y flux, and exhibits a broad plateau between approximately 5×10^{19} cm^{-3} and 2×10^{20} cm^{-3}. Higher carrier concentrations produce a sharp drop in mobility. The increase in mobility is attributed to a reduction of intrinsic donors (i.e., oxygen vacancies) with increasing carrier density while the ultimate decrease in mobility results from a combination of factors including cadmium vacancies, reduced crystal quality, and smaller crystallite sizes, all of which accompany carrier density values greater than the mid 10^{20} cm^{-3} range. This work demonstrates that CdO thin films can be prepared by magnetron sputtering with transport properties and crystal quality that are comparable to those grown using molecular beam epitaxy.
[http://dx.doi.org/10.1063/1.4993799]

In recent years, conductive metal oxides have been increasingly investigated in the context of electronic, plasmonics, and optical technologies. The interest in plasmonic technologies surrounds many emergent optoelectronic applications, such as plasmon lasers,[1] transistors,[2] sensors,[3] and information storage.[4] While plasmonic materials, such as gold and ITO, have been found for ultraviolet-visible and near infrared wavelengths, the mid-infrared range remains a challenge to address due to low free carrier mobility values (i.e., high plasmonic loss) common in conductors with carrier concentrations that support plasmonic resonance in the infrared. Recently, Sachet *et al.* demonstrated electron mobilities surpassing 500 cm^2 V^{-1} s^{-1} at carrier densities greater than 5×10^{19} cm^{-3} in Dy-doped CdO (CdO:Dy). These unique transport properties satisfy the criteria for mid-infrared spectrum plasmonics and overcome the optical losses seen in conventional conductors, such as noble metals.[5] In this work, the precision doping afforded by oxide molecular beam epitaxy enables one to explore and understand the relationships between composition, defect chemistry, and electronic transport in CdO:Dy. However, the sophistication of MBE instrumentation presents a barrier for material implementation. As such, there is interest to explore if similar properties are achievable in alternative deposition methods. Furthermore, there may be additional opportunities for property optimization with techniques that can access non-equilibrium processing conditions and higher pressures and temperatures.

The thin film community explored alternative process methods to manufacture doped cadmium oxide thin films, such as metalorganic vapor phase-epitaxy,[6] pulsed laser deposition,[7] colloidal nanocrystals,[8] and radio frequency sputtering.[9] However, there are no reports that duplicate the reported property trends of CdO:Dy in the similarly low concentration regime ($<1 \times 10^{20}$ cm^{-3}) needed to identify the salient defect chemistry trends. In this work, we demonstrate donor doped CdO films prepared by high-power impulse magnetron sputtering (HiPIMS) where it is possible to combine the material quality of MBE with the practicality and flexibility of a magnetron sputtering infrastructure.

Conventional magnetron sputtering plasmas are sustained by either DC or radio frequency (RF) power, which is typically chosen based on the target resistivity. In the past decade, deposition from

pulsed DC plasmas has gained increasing attention. Using pulsed DC, one can vastly extend the power limitations typically imposed by target melting temperature or the magnetron depoling, provided the durations are short. For example, power densities on the order of 10 W/cm^2 are used commonly to sputter materials like HfO_2, $In_{1-x}Sn_xO_3$, and TiN. This produces ionization fractions on the order of 10%. In many cases, a higher ionization fraction is desired, for example, to increase oxidation in a reactive deposition or to promote additional energetic bombardment. If ionization fractions exceed ~80%, a self-sputter regime can be reached where the bombarding species is primarily the target material (i.e., gasless sputtering).[10] The power densities needed to access this ionization extreme would overheat conventional cathodes if run continuously. They can, however, be sustained when operated in pulsed mode. Imposing a duty cycle where the on time is ~10% and pulse duration is on the order of 100 μs achieves this condition. During these short pulses, power densities ≥ kW/cm^2 can be achieved, leading to high sputter rates, advantageous substrate bombardment, high reactivity, denser as-deposited films, and a reduced surface roughness.[11] The experiments presented below demonstrate that HiPIMS enables one to prepare doped CdO thin films with crystal structure, surface roughness, and transport properties comparable to MBE-grown material and that one can co-deposit a donor dopant using an RF magnetron cathode source.

Heteroepitaxial thin films of CdO:Y (~150 nm) were prepared by reactive HiPIMS from a metallic Cd target (99.9999% metal basis) and by reactive RF sputtering from a metallic Y target (99.9+% metal basis). The magnetrons are oriented slightly outside the confocal point at a horizontal substrate in sputter-down geometry with ~45° angle of incidence. All films were sputtered in an argon-oxygen environment at 10 mTorr flowing 19 SCCM Ar and 13 SCCM O_2. The HiPIMS parameters were 800 Hz and 80 μs pulse time, this produces a 1250 μs period and 6.4% duty cycle. The HiPIMS plasma was driven by a Starfire Industries Impulse Pulsed Power Module and an Advanced Energy MDX 1.5K DC power supply, while the RF plasma was driven by an Advanced Energy RFX-600 and a Manitou Systems manual matching network. The DC power supply that feeds the HiPIMS unit was operated in constant voltage mode with a target value of 400 V. Two-inch diameter MeiVac MAK cathodes were used for both metals.

Doping was achieved by co-sputtering. To modulate the dopant flux and ultimately the carrier concentration in the range of interest, it is necessary to vary both the dopant target-to-substrate distance and the RF power. To quantify these coupled parameters, we introduce the quantity (W/cm^{-4}), which is the time averaged power density applied to the dopant cathode divided by the cathode-to-substrate distance. In the regime of carrier concentrations reported, a deposition rate of approximately 33 nm/min was maintained. Note that increasing the dopant magnetron power density had negligible effect on deposition rate.

All films were grown on epitaxial-polished *c*-plane sapphire substrates bonded to a stainless steel puck using silver paint. For all depositions, the puck surface temperature was 370 °C and monitored by a Raytek 1.6 μm MM Series Pyrometer. All samples were annealed at 700 °C for 1 h in flowing O_2 post-deposition to optimize oxygen uptake.

CdO transport properties were characterized using an Ecopia HMS-3000 Hall Measurement System. Crystal quality and lattice parameters were characterized by X-ray diffraction (XRD) using a Panalytical Empyrean XRD in parallel beam geometry employing a double bounce hybrid monochrometer for the incidence beam optic and a 0.18° parallel plate collimator. Film thickness values were determined by X-ray Reflectivity (XRR).

The signature experiment central to this report monitors the carrier concentration and mobility as a function of Y addition. To do so, a set of CdO films were prepared where the Y flux was increased systematically. Figure 1 summarizes the carrier concentration and mobility trends collected for this series, the most important observations include: (1) intrinsic CdO has a carrier concentration of 1.8 × 10^{19} cm^{-3} and a mobility of 330 cm^2 V^{-1} s^{-1}; (2) carrier concentration increases monotonically with increasing Y flux, up to a maximum value of ~3.3 × 10^{20} cm^{-3}; and (3) mobility increases to a plateau value > 400 cm^2 V^{-1} s^{-1} up to a carrier concentration of ~2.2 × 10^{20} cm^{-3} and falls rapidly as additional yttrium is added.

CdO has a cubic rocksalt structure with a direct and indirect bandgap of approximately 2.2 eV[12] and 0.84 eV,[13] respectively. The conductivity of undoped CdO is attributed to its intrinsic *n*-type behavior where sub-stoichiometric oxygen content promotes oxygen vacancy formation compensated

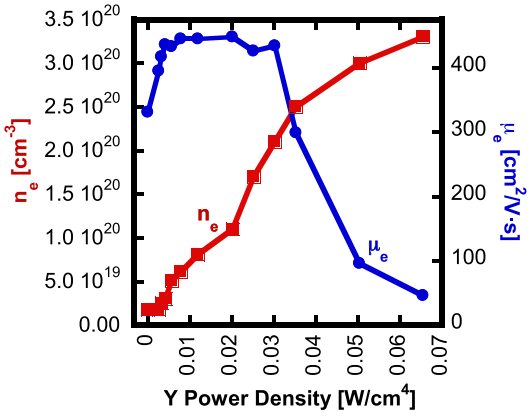

FIG. 1. Carrier concentration (red, square) and mobility (blue, circle) as a function of, coupled, magnetron power density and cathode to substrate distance for donor doped CdO at a thickness of 150 nm.

by electrons. The high carrier concentrations at room temperature can be attributed to their shallow energy level relative to the conduction band minimum. Using hybrid DFT calculations, Burbano *et al.* shows that oxygen vacancies present in intrinsic CdO act as doubly ionized shallow donors, unlike all other *n*-type transparent conducting oxides.[14]

Carrier density increases with increasing Y content and can be attributed to the following defect chemistry reaction for dissolution of Y in a CdO lattice.

$$Y_2O_3 \xrightarrow{CdO} 2Y_{Cd}^{\cdot} + 2O_O^X + 2n + \frac{1}{2}O_2\,(g)\,. \tag{1}$$

For Y-accommodation as a 3^+ cation, its most stable state, every yttrium ion will be compensated by one electron. Between 2×10^{19} cm^{-3} and 2×10^{20} cm^{-3}, the increase in carrier concentration is linear with power density/working distance suggesting a constant activation rate. It is interesting to note that carrier density is essentially flat for very low Y content while in the same range mobility increases sharply. Previous reports for Dy-doped CdO showed that adding aliovalent donors reduced the concentration of oxygen vacancies promoted by a Fermi level shift to larger values, which in turn increased the energetic expense of oxygen vacancy compensation and thus formation.[5] We hypothesize that this initial plateau corresponds to the region where carriers introduced by Y are effectively balanced by a reduction of carriers that compensate oxygen vacancies, thus the flat response. In this same doping region, there is a large increase in electron mobility. As for the case of CdO:Dy, this trend is explained by a reduced population of oxygen vacancy donors and replacement by Y^{3+} donors. Since charged impurity scattering scales with Z^2, one expects less impact from $2N$ donors with a 1^+ charge with respect to the lattice i.e., $Y_{Dy}^{\bullet}$ than from N donors with a 2^+ charge with respect to the lattice, i.e., $V_o^{\bullet\bullet}$.

From carrier densities between 2×10^{19} cm^{-3} and 2.1×10^{20} cm^{-3}, mobility values are greater than 400 cm^2 V^{-1} s^{-1}, with a small reduction towards the high end of this range. Above 2.1×10^{20} cm^{-3}, the rate of free carrier generation per W/cm^4 reduces, and there is a steep drop in mobility. In this carrier density range, one does not expect such strong carrier-carrier scattering, and it is unlikely that the curvature of the band structure changes so abruptly as to increase the effective mass.[15] As such, alternative mechanisms must be present. It has been shown from DFT calculations that the dominating defects present in doped cadmium oxide are a strong function of the Fermi energy.[5] For carrier densities in the 5.0×10^{20} cm^{-3} range, the Fermi level is shifted higher into the conduction band producing a strong Burstein–Moss shift. As such, the formation energy for cadmium vacancies becomes lower than that for oxygen vacancies. Thus, in this range of carrier density, additional Y donors will be compensated by a growing percentage of metal vacancies as opposed to electrons, which will contribute to charged defect scattering.

In addition, it is possible that a change in film structure accompanies this dopant range and promotes additional scattering. To test this hypothesis, we conducted atomic force microscope (AFM)

and four-circle x-ray diffraction analysis to identify trends in crystallinity and surface microstructure as a function of doping level.

For epitaxial growth on *c*-plane sapphire, the preferred crystallographic registry occurs when the (001) plane of CdO is tilted by 23.5 to sapphire (00.1) with a tilt direction parallel to sapphire ⟨10.0⟩, this high-index orientation was reported by Zúñiga-Pérez *et al.*, which corresponds to a (025) CdO plane parallel to the sapphire basal plane.[6] Consequent to the sapphire symmetry, there are three equivalent in-plane orientations of CdO grains. Because of this tilted growth, CdO reflections are only visible to asymmetric or skew-symmetric scans. Figure 2(a) shows a series of asymmetric θ-2θ scans surrounding the (220) CdO reflections as a function of yttrium doping—the (220) peak is chosen for its high relative intensity and because it can be accessed using an asymmetric configuration. There are two observations of interest: the (220) interplanar spacing of 1.656 Å agrees with the bulk value 1.661 Å[16]; and its height and width are affected negligibly by the yttrium content, until the very highest Y concentrations; *A plot of FWHM values for the (220) reflection as a function of carrier concentration* (i.e., *yttrium concentration*) *is presented in the* supplementary material *section.*

A companion sub-set of omega scans for the same CdO:Y doping series are presented in Fig. 2(b), again for the (220) reflections. A distinct trend appears for increasing yttrium concentration. For carrier concentrations less than ~6.5×10^{19} cm^{-3}, the omega scans reveal a consistent FWHM value of 0.30°. Above this range, the values broaden modestly until the very highest concentrations where mosaicity increases sharply. The increase in mosaicity accompanies the precipitous drop in carrier mobility.

Figure 3 displays a (111) phi scan of CdO:Y with intermediate carrier concentration of 6.1×10^{19} cm^{-3}. As reported previously, CdO adopts an in-plane alignment [100] CdO || [01.0]. This produces three individual CdO orientations related by 120°, each exhibiting 1-fold rotational symmetry with respect to the substrate normal. Finally, theta-two theta scans using the Bragg-Brentano geometry and an area detector were collected for CdO thin films with the highest carrier density and may be found in the supplementary material. These optics are most sensitive to small volume fractions of material or crystallites that are highly disordered and thus poor scatterers. We find no evidence for second phase formation.

AFM images were collected for samples across the doping series to compare surface microstructure. A subset of those images are shown in the supplementary material. Most importantly, the surface images reveal a microstructure that is similar in shape and roughness across the series, but there is a dramatic (nearly 10 ×) decrease in grain size that accompanies the decrease in mobility at the highest carrier density level.

While we cannot at this stage separate the extent to which each aspect regulates carrier mobility, we can conclude that a combination of increased mosaic spread of crystallites, an increased population

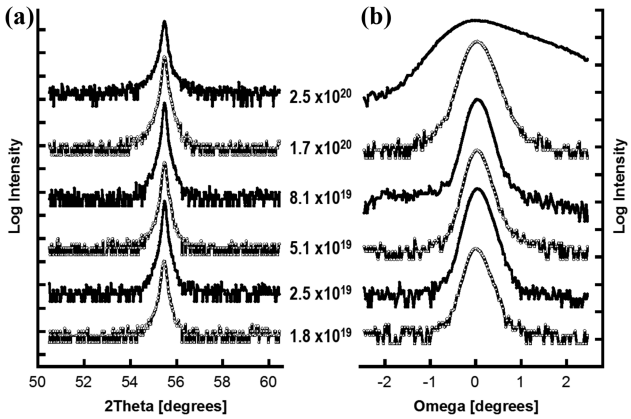

FIG. 2. X-ray diffraction data for a subset of CdO thin films as a function of carrier concentration. (a) Theta-two theta patterns of the (220) reflection show consistently narrow peak widths, while the (b) omega scans show substantial broadening with higher dopant density values.

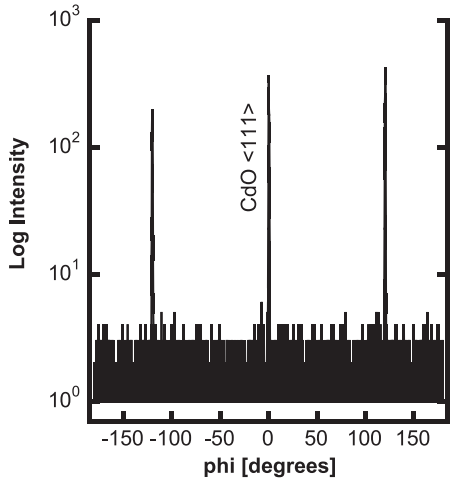

FIG. 3. Phi scan of ⟨111⟩ CdO planes indicating the presence of three equivalent in-plane orientations.

of low angle grain boundaries, and a likely increase in compensating intrinsic defects is responsible for the mobility drop when carrier densities exceed the mid 10^{20} cm^{-3} range. We speculate that these structural trends occur because we are approaching the solubility limit of Y in CdO, where strong crystallographic disorder precedes second phase formation.

Yttrium doped CdO thin films have been grown on *c*-plane sapphire via HiPIMS exhibiting characteristics similar to that of dysprosium doping.[1] The thin films maintain mobility values in the range of 400 cm^2 V^{-1} s^{-1} over the dopant range 1.8×10^{19} cm^{-3} to 3.3×10^{20} cm^{-3}. X-ray diffraction analysis for all films reveals line widths in two-theta that are uniformly narrow and calculated lattice constants that are close to the bulk value. Rocking curve analysis, however, reveals substantial broadening for carrier concentrations above 2.5×10^{20} cm^{-3}. A substantial drop in mobility accompanies this carrier density range. The mobility drop is likely associated with increased crystalline disorder, finer crystallite size, and a cadmium vacancy concentration that is predicted to grow in this dopant regime. MBE-grown CdO:Dy was shown to be a model semiconductor, potentially useful in a variety of applications in the mid-IR spectrum. In this manuscript, we demonstrate that comparable transport properties can be achieved in sputtered CdO with Y donors.

See supplementary material for surface morphology (i.e., AFM images) and additional XRD data (omega FWHM and high resolution long range scan) of the CdO:Y series.

The authors acknowledge support from the National Science Foundation Chemistry Division (No. CHE-1507947), and the Army Research Office (No. W911NF-16-1-0037), and (No. W911NF-16-1-0406). This work was performed in part at the Analytical Instrumentation Facility (AIF) at North Carolina State University, which is supported by the State of North Carolina and the National Science Foundation (Award No. ECCS-1542015). The AIF is a member of the North Carolina Research Triangle Nanotechnology Network (RTNN), a site in the National Nanotechnology Coordinated Infrastructure (NNCI).

[1] R. F. Oulton, V. J. Sorger, T. Zentgraf *et al.*, "Plasmon lasers at deep subwavelength scale," Nature **461**, 629–632 (2009).
[2] H. S. Kojori, J. Yun, Y. Paik, J. Kim, W. A. Anderson, and S. J. Kim, "Plasmon field effect transistor for plasmon to electric conversion and amplification," Nano Lett. **16**(1), 250–254 (2016).
[3] H. Im, H. Shao, Y. Il Park, V. M. Peterson, C. M. Castro, R. Weissleder, and H. Lee, "Label-free detection and molecular profiling of exosomes with a nano-plasmonic sensor," Nat. Biotechnol. **32**(5), 490–495 (2014).
[4] S. Fu, X. Zhang, Q. Han, S. Liu, X. Han, and Y. Liu, "Blu-ray-sensitive localized surface plasmon resonance for high-density optical memory," Sci. Rep. **6**, 36701 (2016).
[5] E. Sachet *et al.*, "Dysprosium-doped cadmium oxide as a gateway material for mid-infrared plasmonics," Nat. Mater. **14**, 414–442 (2015).
[6] J. Zúñiga-Pérez, C. Martínez-Tomás, and V. Muñoz-Sanjosé, "X-ray characterization of CdO thin films grown on *a*-, *c*-, *r*- and *m*-plane sapphire by metalorganic vapour phase-epitaxy," Phys. Status Solidi C **2**, 1233–1238 (2005).
[7] L. L. Pan *et al.*, "Structural, optical and electrical characterization of gadolinium and indium doped cadmium oxide/p-silicon heterojunctions for solar cell applications," RCS Adv. **4**, 52451 (2014).

[8] G. Garcia *et al.*, "Dynamically modulating the surface plasmon resonance of doped semiconductor nanocrystals," Nano Lett. **11**, 4415–4420 (2011).
[9] B. Saha *et al.*, "Wide range tuning of electrical conductivity of RF sputtered CdO thin films through oxygen partial pressure variation," Sol. Energy Mater. Sol. Cells **92**, 1077–1080 (2008).
[10] J. Andersson and A. Anders, "Gasless sputtering: Opportunities for ultraclean metallization, coatings in space, and propulsion," Appl. Phys. Lett. **92**, 221503 (2008).
[11] J. T. Gudmundsson, N. Brenning, D. Lundin, and U. Helmersson, "High power impulse magnetron sputtering discharge," J. Vac. Sci. Technol., A **30**, 030801 (2012).
[12] S. Vasheghani Fahrahani, T. D. Veal, P. D. C. King, J. Zúñiga-Pérez, V. Muñoz-Sanjoé, and C. F. McConville, "Electron mobility in CdO films," J. Appl. Phys. **109**, 073712 (2011).
[13] F. P. Koffyberg, "Thermoreflectance spectra of CdO: Band gaps and band-population effects," Phys. Rev. B **13**(10), 4470 (1976).
[14] M. Burbano *et al.*, "Sources of conductivity and doping limits in CdO from hybrid density functional theory," J. Am. Chem. Soc. **133**(38), 15065–15072 (2011).
[15] J. M. Dorkel and Ph. Leturcq, "Carrier mobilities in silicon semi-empirically related to temperature, doping and injection level," Solid-State Electron. **24**(9), 821–825 (1981).
[16] T. Swanson, Natl. Bur. Stand. (U. S.), Circ. 539 **II**, 27 (1953).